Available online at www.sciencedirect.com
ScienceDirect
Trans. Nonferrous Met. Soc. China 21(2011) 257−264
Transactions of Nonferrous Metals Society of China
www.tnmsc.cn

Hot workability of as-cast and extruded ZE41A magnesium alloy using processing maps

S. ANBU SELVAN, S. RAMANATHAN

Department of Manufacturing Engineering, Annamalai University, Annamalai Nagar, TamilNadu, 608002, India

Received 3 March 2010; accepted 4 May 2010

Abstract: The hot deformation behavior and microstructure evolution of as-cast and extruded ZE41A magnesium alloy were studied using processing maps. The compression tests were conducted on both as-cast and extruded alloys in the temperature range of 250−450 °C and strain rate range of 0.001−1.0 s^{-1} to establish the processing map. The dynamic recrystallization (DRX) and instability zones were identified and validated through micrographs. The extruded ZE41A magnesium alloy shows higher flow stress, higher efficiency and lower instability regimes than as-cast alloy. The extruded ZE41A magnesium alloy achieves good hot workability due to grain refinement, decrease in porosity, hardening and strengthening of the material.
Key words: magnesium alloy; extrusion; processing map; hot workability

1 Introduction

In recent years, the structural applications of magnesium alloys in aerospace and automobile industries are increasing progressively. This is not only because of their lower densities but also because of their excellent properties, such as heat dissipation, damping, electro-magnetic shielding and recycling[1−3]. The inherently poor workability of magnesium and several of its alloys is due to the limited number of slip systems associated with the HCP crystal structure. This restricts the utility of these alloys mostly to the as-cast condition. Although there are several studies addressing the issues specific to superplastic deformation in the commercial wrought magnesium alloys[4]. It is tempting to use the refined grain structure of the magnesium alloy in order to enhance their mechanical properties including ductility and strength[5]. Besides, fine-grained Mg alloy possesses better ductility, as well as, lower ductile brittle transition temperature (DBTT), thus its formability at room temperature can be improved. A fine-grained material is harder and stronger than coarsely grained material because it has a greater total grain boundary area to impede dislocation motion[6]. In the 1970s, it was first reported that the magnesium alloy with high zinc revealed good creep resistance and good die castability[7]. In recent years, new magnesium alloys have been proposed through incorporating rare-earth elements to improve their characteristics for different applications[8]. Rare earth (RE) has many merits, such as purifying alloy melt, modifying castability, refining the microstructure, improving the mechanical properties and anti-oxidization properties. Therefore, RE has been used in magnesium alloys for many years, such as Mg-Zn-RE-Zr[9]. Zirconium addition to rare-earth containing magnesium alloys has been shown to improve the mechanical properties due to grain refinement[10−11].

BEER and BARNETT[12] have studied the hot compression test for as-cast and wrought AZ31 Mg alloy. Their study revealed that the dynamically recrystallized (DRX) grain size of wrought magnesium alloy was lower than that of as-cast magnesium alloy. Also the increasing rate of dynamic recrystallization in the as-cast material was considerably lower than that in the wrought material. LEE et al[13] have assessed the hot workability of as-cast and forged Ti-8Ta-3Nb using processing maps. They concluded that the forged specimen showed higher flow stress than as-cast specimen in the temperature range of 650−900 °C and strain rate range of 0.001−10 s^{-1}. Also the efficiency of the forged specimen was higher than that of as-cast specimen over all the ranges. PRASAD and RAO[14] have reported the hot working

Corresponding author: S. ANBU SELVAN; Tel: +91-9865387907; Fax: +91-4144-239734; E-mail: anbushankari@yahoo.co.in
DOI: 10.1016/S1003-6326(11)60707-3

behaviors of as-cast and homogenized AZ31 Mg alloys using processing maps. They concluded that the homogenization treatment improved hot workability by expanding the workability domains and reducing the flow instability regimes. ZHENG et al[15] have investigated the compressive deformations of as-extruded and equal channel angular pressing (ECAP) Mg-Zn-Y-Zr alloys. They reported that the ECAP-processed alloy exhibited finer grains and higher strain rate sensitivity exponent than as-extruded alloy.

The aim of the present investigation is to compare the hot workabilities of as-cast and extruded ZE41A magnesium alloys through processing maps and microstructural observations. The technique of processing maps was based on the dynamic model of materials, the principles of which were described earlier[16−18]. Briefly, the work-piece undergoing hot deformation is considered to be a dissipator of power and the total power dissipated instantaneously is given by

$$P=\int_0^{\dot{\varepsilon}}\sigma \mathrm{d}\dot{\varepsilon}+\int_0^{\sigma}\dot{\varepsilon}\mathrm{d}\sigma=G+J \tag{1}$$

where σ is the flow stress and $\dot{\varepsilon}$ is the strain rate. In terms of physical systems terminology, the first integral is called G content representing deformation heat and the second one a J co-content, which is a complementary part of G content, representing microstructural dissipation. The strain rate sensitivity (m) of flow stress is the factor that partitions power between deformation heat and microstructural changes since

$$\frac{\mathrm{d}J}{\mathrm{d}G}=\frac{\dot{\varepsilon}\mathrm{d}\sigma}{\sigma\mathrm{d}\dot{\varepsilon}}=\frac{\dot{\varepsilon}\sigma\mathrm{d}\ln\sigma}{\sigma\dot{\varepsilon}\mathrm{d}\ln\dot{\varepsilon}}\approx\frac{\Delta\lg\sigma}{\Delta\lg\dot{\varepsilon}}=m \tag{2}$$

The efficiency of power dissipation (η) occurring through microstructural changes during deformation is derived by comparing the non-linear power dissipation occurring instantaneously in the work-piece with that of a linear dissipater (m=1) and is given by

$$\frac{\Delta J/\Delta P}{(\Delta J/\Delta P)_{\text{linear}}}=\frac{m/(m+1)}{1/2}=\frac{2m}{m+1}=\eta \tag{3}$$

The power dissipation map represents the three-dimensional variation of efficiency with temperature and strain rate which is generally viewed as an iso-efficiency contour map. Further, the extremum principles of irreversible thermodynamics as applied to continuum mechanics of large plastic flow [19] are explored to define a criterion for the onset of flow instability given by the equation for the instability parameter $\xi(\dot{\varepsilon})$:

$$\xi(\dot{\varepsilon})=\frac{\partial\ln[m/(m+1)]}{\partial\ln\dot{\varepsilon}}+m\le 0 \tag{4}$$

In simple terms, the material will exhibit flow instability if the rate of internal entropy production generated by the system during hot deformation is lower than that imposed by the applied processing parameters. The variation of the instability parameter as a function of temperature and strain rate represents an instability map which delineates regimes of instability, where ξ is negative. A superimposition of the instability map on the power dissipation map gives a processing map which reveals domains (efficiency contours converging towards a peak efficiency), where individual microstructural processes dominate and the limiting conditions for the regimes (bounded by a contour for ξ =0) of flow instability. Processing maps help in identifying temperature-strain rate windows for hot working, where the intrinsic workability of the material is the maximum (e.g. dynamic recrystallization (DRX) or superplasticity) and also in avoiding the regimes of flow instabilities (e.g. adiabatic shear bands or flow localization) or cracking. The processing map technique has been used earlier to study the hot deformation mechanisms in magnesium and its alloys[4, 20−24] including dynamic recrystallization (DRX) and flow instabilities.

2 Experimental

The chemical composition (mass fraction, %) of the ZE41A magnesium alloy was as follows: 3.85Zn, 1.27Ce, 0.53Zr, 0.002Cu, 0.006Al, 0.008Mn, 0.004Fe, 0.003Si, 0.002Ni and the rest Mg. The as-cast material was machined into 31 mm in diameter and 50 mm in length and then extruded at 300 °C with a rate of 4 m/min to give solid bars with diameter of 17 mm corresponding to a reduction ratio in area of 70%. Cylindrical specimens of 10 mm in diameter and 10 mm in height were machined for compression test from the as-cast and extruded ingots. For inserting a thermocouple to measure the specimen temperature as well as the adiabatic temperature rise during deformation, the specimens were provided a hole with 0.8 mm in diameter machined at mid height to reach the centre of the specimen.

The initial microstructures of as-cast and extruded ZE41A magnesium alloys are shown in Figs.1(a) and (b), respectively. Also the mechanical properties of as-cast and extruded alloys are shown in Table 1. Isothermal uniaxial compression tests were conducted at constant true strain rates in the range of 0.001−1.0 s^{-1} and temperature range of 250−450 °C for both alloys, as shown in Fig.2. The specimens as well as the push rods holding the platens were heated in a clam-shell furnace to the required temperature and held at that temperature for 10 min before starting the compression test. The temperature of the specimen and the adiabatic temperature rise were monitored during the test using the thermocouple embedded in the specimen. Constant true

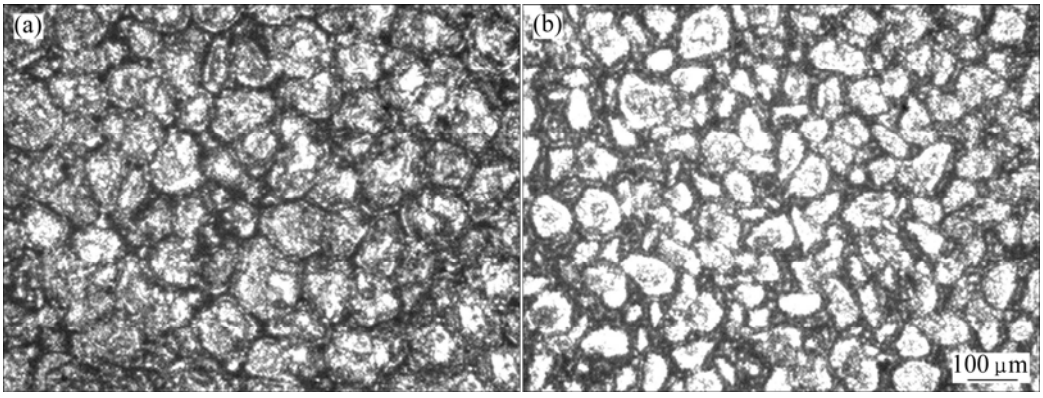

Fig.1 Initial microstructures of ZE41A magnesium alloys: (a) As-cast specimen; (b) Extruded specimen

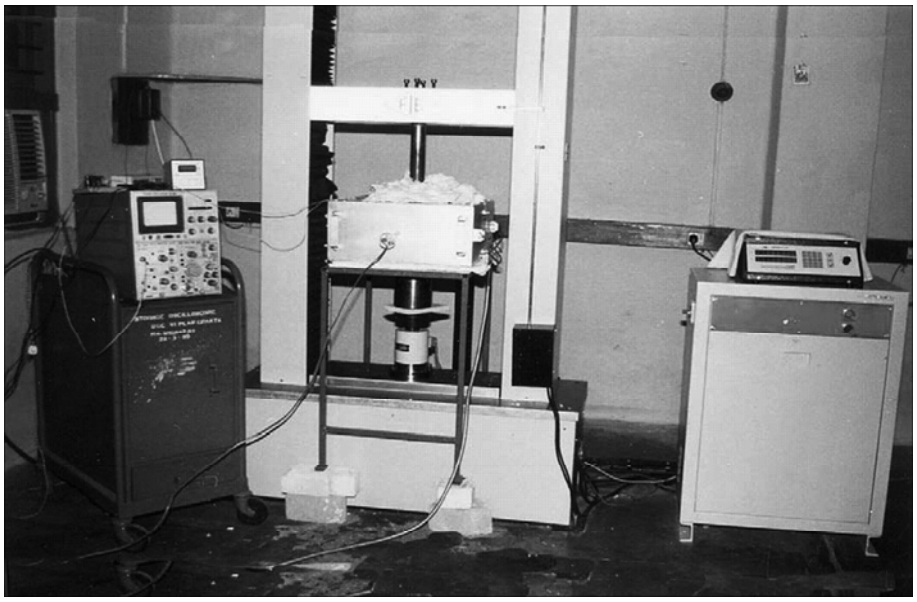

Fig.2 Servo controlled universal testing machine used for hot compression test

Table 1 Mechanical properties of as-cast and extruded ZE41A magnesium alloys

Material	Grain size/ μm	Microhardness, HV	UTS/ MPa	Ductility/ %
As-cast alloy	78.2 ± 5	65.1 ± 0.3	206.1 ± 4	4.6 ± 0.2
Extruded alloy	41.3 ± 4	74.5 ± 0.6	310.3 ± 2	3.2 ± 0.3

strain rates in the servo hydraulic machine were achieved during the tests by a computer control that gives an exponential decay of actuator speed. Graphite power mixed with grease was used as the lubricant in all experiments. The specimens were deformed up to a true strain of 0.5 and then quenched in water. The load-stroke data were converted into true stress—true strain curves using standard equations. The flow stress values were corrected for adiabatic temperature rise by assuming linear relationship between logarithm of flow stress and inverse of temperature within the intervals of experimental data points. The strain rate sensitivities of flow stress (Eq.(2)) at different strain rates for each test temperature were estimated by fitting a spline function to flow stress—strain rate data and the procedure repeated at the various test temperatures. The efficiency of power dissipation (η) was then calculated by plugging the estimated m values in Eq.(3) and plotted against temperature and strain rate to obtain a three-dimensional power dissipation map and a contour map. The instability criterion given by Eq.(4) was evaluated using the above m values and plotted over the power dissipation map for marking the limiting condition where ξ=0. The deformed specimens were sectioned in the center parallel to the compression axis and the cut surface was mounted, polished and etched for metallographic examination. All the specimens were etched with an aqueous solution containing 10% picric acid.

3 Results and discussion

3.1 Interpretation from flow curves

Fig.3 shows the flow curves of as-cast and extruded ZE41A magnesium alloys deformed at 400 °C and different strain rates ranging from 0.001 to 1.0 s^{-1}. Fig.4 shows the flow curves of as-cast and extruded ZE41A magnesium alloys deformed at 0.1 s^{-1} and different temperatures ranging from 250 to 450 °C. From the stress—strain curves, it is observed that the flow stress of extruded alloy is higher than that of as-cast alloy over the temperatures and strain rates. This is achieved by grain refinement of the extruded alloy. A fine-grained material is harder and stronger than coarsely grained material because it has a greater total grain boundary area to impede dislocation motion[6]. In Table 1, it is clearly mentioned that the strength and hardness of extruded alloy are higher than those of as-cast alloy. Also the grain size of ZE41A magnesium alloy is reduced from 78.2 μm to 41.3 μm due to extrusion. Therefore, the flow stress values of extruded ZE41A magnesium alloy are higher than those of as-cast alloy due to the decrease in grain size, increase in strength and hardness. For both as-cast and extruded alloys the flow stress increased rapidly before softening occurred and flow softening is significant at lower temperatures and higher strain rates. The curves tend to exhibit steady state flow at lower strain rates and higher temperatures for both alloys.

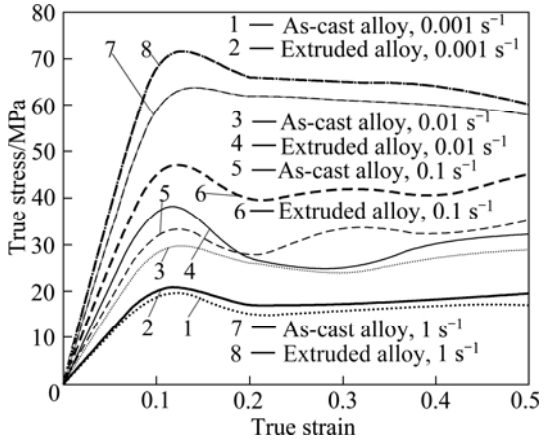

Fig.3 True stress—strain curves obtained for as-cast and extruded ZE41A magnesium alloy deformed at 400 °C and various strain rates

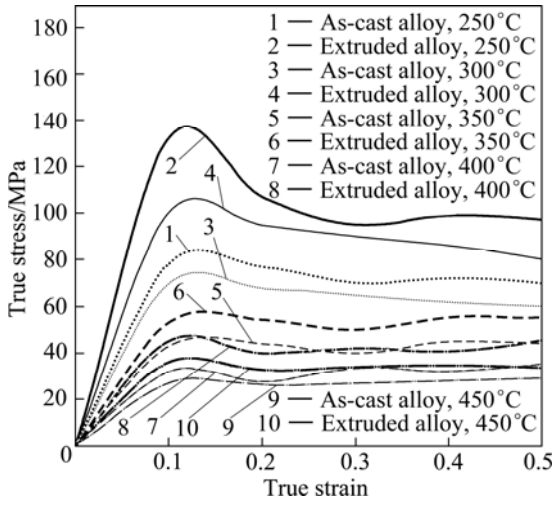

Fig.4 True stress—strain curves obtained for as-cast and extruded ZE41A magnesium alloy deformed at 0.1 s^{-1} and various temperatures

3.2 Interpretation from processing maps

The processing maps for as-cast and extruded ZE41A magnesium alloys obtained by superimposing the instability map on the efficiency map for 0.5 of strain are shown in Fig.5 and Fig.6, respectively. The contour numbers represent power dissipation efficiency and the shaded domains indicate the regions of flow instability (negative flow instability parameter). In the processing map of as-cast alloy (Fig.5), there exists a domain in the temperature of 330−380 °C, strain rate of 0.01−0.1 s^{-1}, having a maximum efficiency of 34%, while it exists in the extruded alloy (Fig.6) in the temperature of 390−430 °C, strain rate of 0.02−0.1 s^{-1} and having a maximum efficiency of 44%. Fig.7(a) shows the micrograph of as-cast alloy deformed at 350 °C and 0.1 s^{-1}. Fig.7(b) shows the micrograph of extruded alloy deformed at 400 °C and 0.1 s^{-1}. The above microstructures have three features as follows: 1) equiaxed grain forms in the band structure by compression; 2) grain size is fine compared with initial grain size, it is indicative of refinement of grain; and 3) grain boundaries are irregular or wavy in nature. These features agree well with DRX[22]. The above domain represents complete DRX process which is desirable and 'safe' for processing. This conforms to earlier studies by JAGAN et al[25], RAGHUNATH et al[26] and GANESAN et al[27]. During DRX, subgrains

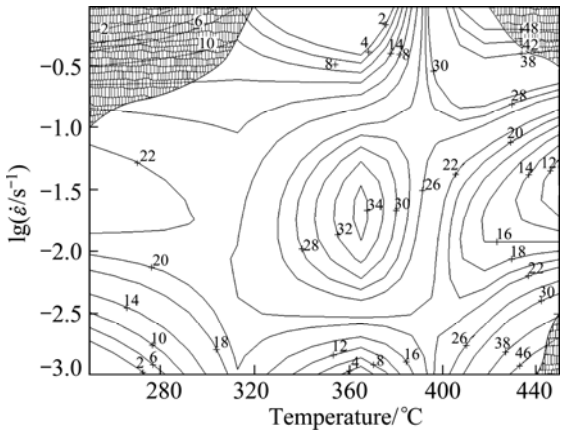

Fig.5 Processing map of as-cast ZE41A magnesium alloy at strain of 0.5

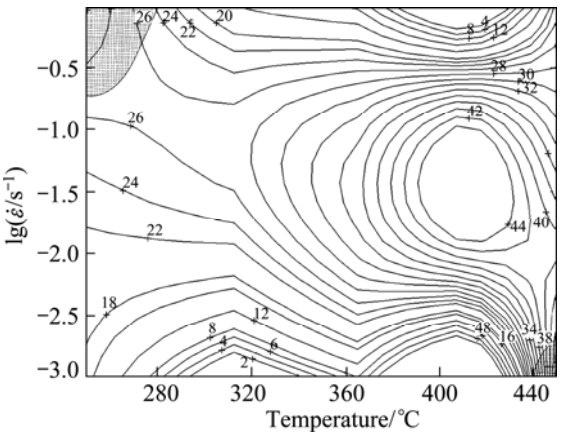

Fig.6 Processing map of extruded ZE41A magnesium alloy at strain of 0.5

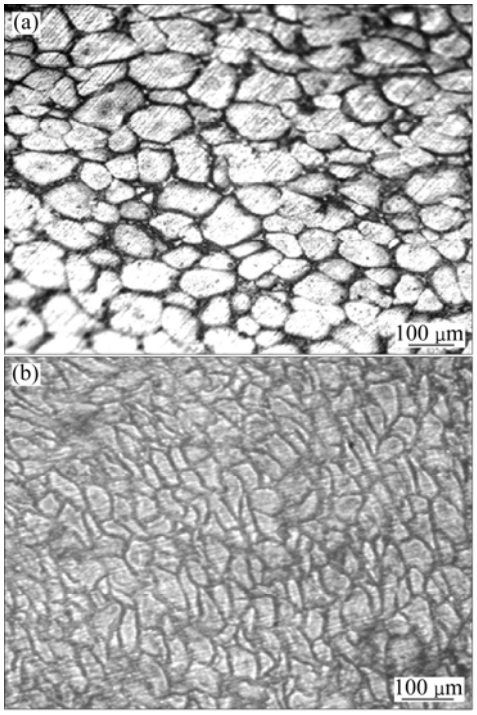

Fig.7 Microstructures showing dynamic recrystallization for as-cast alloy at 350 °C and 0.1 s^{-1} (a) and extruded alloy at 400 °C and 0.1 s^{-1} (b)

are first developed in the vicinity of the serrated grain boundaries and as deformation progresses, subgrain structure will form over the whole volume of the grain through the conversion of dislocation cell walls into subgrain boundaries[28]. By comparing Figs.7(a) and (b), it is observed that the dynamically recrystallized grain size of the extruded alloy is smaller than that of as-cast alloy. This is achieved by grain refinement, decrease in porosity, hardening and strengthening of the alloy by hot extrusion. This is well agreed with CHANDRASEKARAN and JOHN[29] and EL-MORSY et al[6]. Hence, the optimum conditions for hot working of as-cast ZE41A magnesium alloy in the safe domain are 360 °C and 0.05 s^{-1} with a maximum efficiency of 34%. Also the optimum conditions for hot working of extruded ZE41A magnesium alloy in the safe domain are 400 °C and 0.1 s^{-1} with a maximum efficiency of 44%. The maximum power dissipation efficiency in the DRX domain of the extruded alloy is higher than that of as-cast alloy. This is because of the strengthening effect. Similar findings were reported by LEE et al[13].

3.3 Instability zones

3.3.1 Flow localization

The adiabatic shear bands occur during compression in the range of 250−320 °C and 0.1−1.0 s^{-1} for as-cast alloy, as shown in Fig.5. Also for extruded alloy, the adiabatic shear bands occur in the range of 250−280 °C and 0.32−1.0 s^{-1}, as shown in Fig.6. These predictions are further validated by the microstructural observations on the deformed specimens[30]. Figs.8(a) and (b) show the micrographs of as-cast and extruded alloys deformed at 250 °C and 1.0 s^{-1}, respectively. Adiabatic shear bands can be observed at an angle of about 45° to the compressive axis. The regions, where the microstructure reveals intense adiabatic shear bands, macro-structure shows cracks in the maximum shear stress plane, negative strain rate sensitivity, higher work hardening rate, higher rise in the specimen temperature during deformation and higher flow stress, are observed and are marked as regimes of adiabatic shear deformation[31]. The adiabatic shear bands occurred in lower temperature and in higher strain rate regions[24]. At higher strain rates, heat generated due to local temperature rise by plastic deformation is not conducted away to the cooler regions of the body since the available time is too short. The flow stress in deformation band will lower and further plastic flow will be localized. The band gets intensified and nearly satisfies adiabatic conditions. Such bands are called adiabatic shear bands (ASB) which exhibit cracking, recrystallization or phase transformation along macroscopic shear planes[32]. Fig.9(a) shows that the microstructure of extruded alloy consists of twining and bands of flow localization at 250 °C and 1.0 s^{-1}, which should be described as unstable deformation regions corresponding to instability maps[22]. Compression twins are immobile and cannot carry the whole strain within very limited volume. Therefore, compression twins contribute little to plasticity but are prone to initiate cracks[33]. The occurrence of twinning at low temperatures or high strain rates in HCP metals at orientations is unfavorable for basal slip[34]. Fig.9(b) shows the formation of cracks in shear bands at 250 °C and 1.0 s^{-1} in the extruded alloy. These temperatures and strain rates should be avoided in processing the materials. By comparing the flow

localization area of both alloys, the extruded alloy has lower instability region than as-cast alloy.

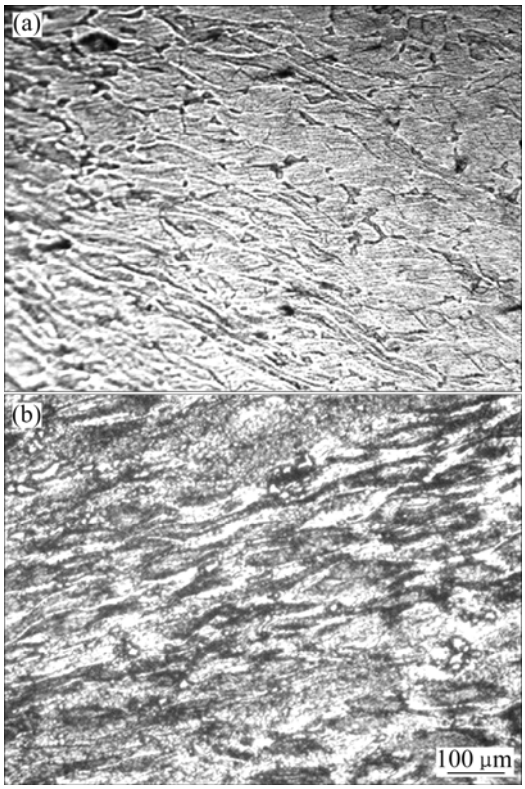

Fig.8 Microstructures showing adiabatic shear bands deformed at 250 °C and 1.0 s^{-1} for as-cast alloy (a) and extruded alloy (b)

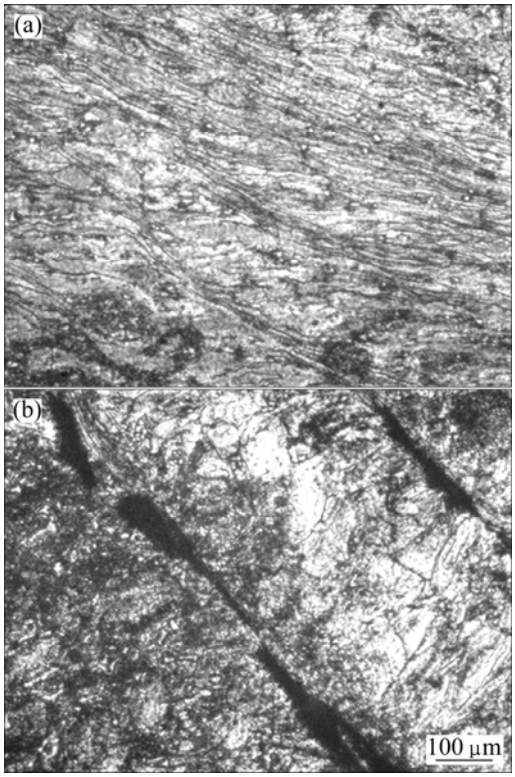

Fig.9 Microstructures of extruded alloy deformed at 250 °C and 1.0 s^{-1} showing twinning (a) and cracks (b) in adiabatic shear bands

3.3.2 Wedge cracking

From Fig.5 and Fig.6, wedge cracks can be observed for as-cast alloy in the range of 440−450 °C and 0.001−0.005 s^{-1}, while for extruded alloy in the range of 440−450 °C and 0.001−0.003 s^{-1}. The microstructures of as-cast and extruded alloys deformed at 450 °C and 0.001 s^{-1} are shown in Figs.10(a) and (b) respectively. According to RAJ[35], the domain occurring at higher temperatures and lower strain rates represents the process of grain boundary sliding. The stress concentrations occurring at the grain boundary triple junctions, if not relieved by accommodation process, will result in wedge cracking. At low strain rates and higher temperatures, grain boundary sliding occurs under shear stress where the diffusion rates are not fast enough, wedge cracking occurs at the grain boundary junctions. The state of stress will have a significant influence on the manifestation of these cracks. Wedge cracking is reduced by increasing the strain rate or decreasing the temperature, both of which reduce the extent of grain boundary sliding. This is conformed by GANESAN et al[27]. These domains should be avoided in processing the materials. By comparing these domains for both alloys, the extruded alloy has lower instability region than as-cast alloy.

3.3.3 Matrix cracking

For as-cast alloy, matrix crack occurs in the range of 420−450 °C and 0.5−1.0 s^{-1}as shown in Fig.5. The microstructure of as-cast alloy deformed at 450 °C and 1.0 s^{-1} is shown in Fig.11. The flow of matrix that occurs at high temperatures causes large local stresses, resulting in deformation and breakage. As the temperature increases, this stress would cause local plastic deformation. When the stress is higher than the fracture strain, the material would crack, resulting in complete failure. This agrees with the findings of WANG et al[36]. So these conditions should be avoided in processing the material.

4 Conclusions

1) The temperature and strain rate significantly affect the flow stress in the isothermal deformation of both as-cast and extruded ZE41A magnesium alloys. The flow stress decreases with the increase of deformation temperature and decrease of strain rate for both as-cast and extruded materials.

2) The flow stress of the extruded alloy shows higher than that of as-cast alloy over the ranges of temperatures and strain rates.

3) The maximum power dissipation efficiency in the DRX domain of extruded alloy is higher than that in as-cast alloy.

4) The extruded alloy shows reduced flow instability regimes as compared with as-cast alloy.

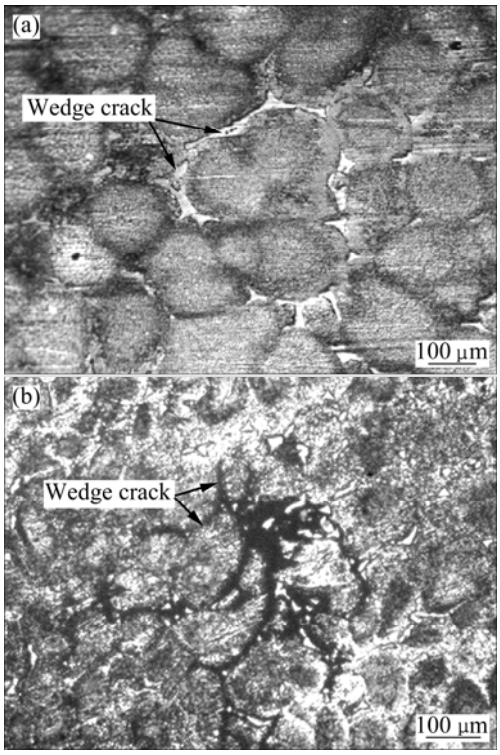

Fig.10 Microstructures showing wedge crack deformed at 450 °C and 0.001 s^{-1} for as-cast alloy (a) and extruded alloy (b)

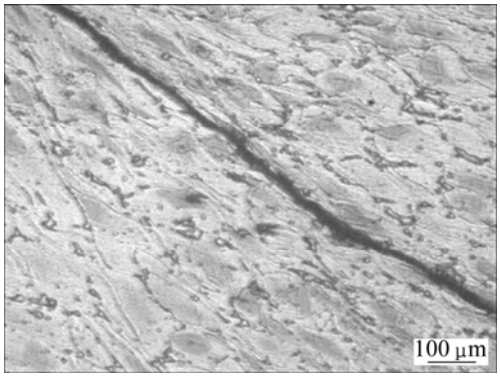

Fig.11 Microstructure showing matrix crack in as-cast alloy deformed at 450 °C and 1.0 s^{-1}

5) The extruded ZE41A magnesium alloy has improved hot workability as compared with as-cast alloy due to grain refinement, decrease in porosity, hardening and strengthening of the material.

Acknowledgements

The authors are grateful to Hindustan Aeronautic Limited (HAL), Bangalore, India for providing material and technical assistance.

References

[1] LEE S, CHEN Y H, WANG J Y. Isothermal sheet formability of magnesium alloy AZ31 and AZ61 [J]. Journal of Material Processing Technology, 2002, 124: 19−24.

[2] TAKUDA H, ENAMI T, KUBOTA K. The formability of a thin sheet of Mg-8.5Li-1Zn alloy [J]. Journal of Material Processing Technology, 2000, 101: 281−286.

[3] TAKUDA H, FUJIMOTO H, HATTA N. Modelling of flow stress of Mg-Al-Zn alloys at elevated temperatures [J]. Journal of Material Processing Technology, 1998, 80: 513−516.

[4] SRINIVASAN N, PRASAD Y V R K, RAMA RAO P. Hot deformation behavior of Mg-3Al alloy [J]. Materials Science and Engineering A, 2008, 476: 146−156.

[5] TAKAMURA H, MIYASHITA T, KAMEGAWA A, OKADA M. Grain size refinement in Mg-Al-based alloy by hydrogen treatment [J]. Journal of Alloys and Compounds, 2003, 356: 804-808.

[6] EL-MORSY A, ISMAIL A, WALY M. Microstructural and mechanical properties evolution of magnesium AZ61 alloy processed through a combination of extrusion and thermomechanical processes [J]. Materials Science and Engineering A, 2008, 486: 528−533.

[7] KING J F. Mg alloys and their applications [M]. Wolfsburg, 1998: 37− 47.

[8] LI Q, WANG Q D, WANG Y X, ZENG X Q, DING W J. Effect of Nd and Y addition on microstructure and mechanical properties of as-cast Mg-Zn-Zr alloy [J]. Journal of Alloys and Compounds, 2007, 427: 115−123.

[9] WEI L Y, DUNLOP G L, WESTENGEN H. The intergranular microstructure of cast Mg-Zn and Mg-Zn-rare earth alloys [J]. Metallurgical and Materials Transactions A, 1995, 26: 1947−1955.

[10] BEN-HAMU G, ELIEZER D, SHIN K S, COHEN S. The relation between microstructure and corrosion behavior of Mg-Y-RE-Zr alloys [J]. Journal of Alloys and Compounds, 2007, 431: 269−276.

[11] YANG Z, GUO Y C, LI J P, HE F, XIA F, LIANG M X. Plastic deformation and dynamic recrystallization behaviors of Mg-5Gd-4Y-0.5Zn-0.5Zr alloy [J]. Materials Science and Engineering A, 2008, 485: 487−491.

[12] BEER A G, BARNETT M R. Microstructural development during hot working of Mg-3Al-1Zn [J]. Metallurgical and Materials Transactions A, 2007, 38: 1856−1867.

[13] LEE K W, BAN J S, LEE M G, KIM G H, CHO K Z. Processing map for the hot working of Ti-8Ta-3Nb [J]. Journal of Mechanical Science and Technology, 2008, 22: 931−936.

[14] PRASAD Y V R K, RAO K P. Effect of homogenization on the hot deformation behavior of cast AZ31 magnesium alloy [J]. Materials and Design, 2009, 30: 3723−3730.

[15] ZHENG M Y, XU S W, QIAO X G, WU K, KAMADO S, KOJIMA Y. Compressive deformation of Mg-Zn-Y-Zr alloy processed by equal channel angular pressing [J]. Materials Science and Engineering A, 2008, 483: 564−567.

[16] PRASAD Y V R K, SHESHACHARULU T. Modelling of hot deformation for microstructural control [J]. International Materials Reviews, 1998, 44: 243−258.

[17] PRASAD Y V R K, SASIDHARA S. Hot working guide for a compendium of processing maps [M]. Russell Township: ASM International, Materials Park, 1997.

[18] PRASAD Y V R K. Processing maps: A status report [J]. Journal of Materials Engineering and Performance, 2003, 12: 638−645.

[19] ZIEGLER H. Progress in solid mechanics [M]. New York: Wiley, 1965: 91.

[20] DZWONCZYK J, PRASAD Y V R K, HORT N, KAINER K U. Enhancement of workability in AZ31 alloy—Processing maps: Part I, Cast material [J]. Advanced Engineering Materials, 2006, 8: 966−973.

[21] WANG Y, ZHANG Y, ZENG X, DING W. Characterization of dynamic recrystallisation in as-homogenized Mg-Zn-Y-Zr alloy using processing map [J]. Journal of Materials Science, 2006, 41: 3603−3608.

[22] WANG C Y, WANG X J, CHANG H, WU K, ZHENG M Y. Processing maps for hot working of ZK60 magnesium alloy [J]. Materials Science and Engineering A, 2007, 464: 52−58.
[23] SIVAKESAVAM O, RAO I S, PRASAD Y V R K. Processing map for hot working of as cast magnesium [J]. Materials Science and Technology, 1993, 9: 805−810.
[24] SIVAKESAVAM O, PRASAD Y V R K. Hot deformation behavior of as-cast Mg-2Zn-1Mn alloy in compression: A study with processing map [J]. Materials Science and Engineering A, 2003, 362: 118−124.
[25] JAGAN R G, SRINIVASAN N, GOKHALE A A, KASHYAP B P. Processing map for hot working of spray formed and hot isostatically pressed Al-Li alloy (UL40) [J]. Journal of Materials Processing Technology, 2009, 209: 5964−5972.
[26] RAGHUNATH B K, KARTHIKEYAN R, GUPTA M. An investigation of hot deformation response of particulate-reinforced magnesium + 4.5% titanium composite [J]. Materials Research, 2006, 9: 217−222.
[27] GANESAN G, RAGHUKANDAN K, KARTHIKEYAN R, PAI B C. Development of processing maps for 6061 Al/15% SiCp composite material [J]. Materials Science and Engineering A, 2004, 369: 230−235.
[28] TAN J C, TAN M J. Dynamic continuous recrystallization characteristics in two stage deformation of Mg-3Al-lZn alloy sheet [J]. Materials Science and Engineering A, 2003, 339: 124−132.
[29] CHANDRASEKARAN M, JOHN Y M S. Effect of materials and temperature on the forward extrusion of magnesium alloys [J]. Materials Science and Engineering A, 2004, 381: 308−319.
[30] LI A B, HUANG L J, MENG Q Y, GENG L, CUI X P. Hot working of Ti-6Al-3Mo-2Zr-0.3Si alloy with lamellar $\alpha + \beta$ starting structure using processing map [J]. Materials and Design, 2009, 30: 1625−1631.
[31] VENUGOPAL S, VENUGOPAL P, MANNAN S L. Optimisation of cold and warm workability of commercially pure titanium using dynamic materials model (DMM) instability maps [J]. Journal of Materials Processing Technology, 2008, 202: 201−215.
[32] RAMANATHAN S, KARTHIKEYAN R, GUPTA M. Development of processing maps for Al/SiC_p composite using fuzzy logic [J]. Journal of Materials Processing Technology, 2007, 183: 104−110.
[33] YANG Ping. Dependency of deformation twinning on grain orientation in an FCC and a HCP metal [J]. Frontiers of Materials Science in China, 2007, 1: 331−341.
[34] DIETER E. Mechanical metallurgy [M]. London: McGraw-Hill Press, 1988.
[35] RAJ R. Development of a processing map for use in warm-forming and hot-forming process [J]. Metallurgical and Materials Transactions A, 1981, 12: 1089−1097.
[36] WANG C Y, WU K, ZHENG M Y. Hot deformation and processing maps of $Al_{18}B_4O_{33}w$/ZK60 composite [J]. Materials Science and Engineering A, 2008, 477: 179−184.

用热加工图研究铸态和挤压态 ZE41A 镁合金的热加工性能

S. ANBU SELVAN, S. RAMANATHAN

Department of Manufacturing Engineering, Annamalai University,
Annamalai Nagar, TamilNadu, 608002, India

摘　要：采用热加工图研究铸态和挤压态 ZE41A 镁合金的热变形行为和组织演变。在温度 250−450 °C，应变速率 0.001−1.0 s^{-1} 的条件下，对铸态和挤压态合金进行抗压测试，建立热加工图。通过显微组织观察确定动态再结晶和不稳定区域。挤压态 ZE41A 镁合金比铸态合金具有较高的流变应力，较高的能量损耗率和较小的不稳定区域。由于晶粒的细化、材料孔隙度的降低、硬化和强化，挤压态镁合金具有良好的热加工性能。

关键词：镁合金；挤压；加工图；热加工性

(Edited by LI Xinag-qun)